Progress In Electromagnetics Research C, Vol. 126, 173–181, 2022

Design and Fabrication of Adjustable Reflectionless Microstrip Diplexer for L-Band

Abbas Taghvaei, Reza Bayderkhani*, and Maryam Espahbodi

Abstract—In this study, an adjustable reflectionless diplexer is designed and fabricated for the L-band based on microstrip transmission lines. The proposed diplexer can separate and combine different frequencies within the L-band frequency range. The equations and theoretical process of the structure can be proved from coupling matrix and even/odd mode circuit analysis. In this design, our aim is that the proposed diplexer not only has low insertion loss and proper return loss in the channels' stopband but also can change the channels' frequency. The physical specifications are calculated proportionally to the central frequency based on the coupling coefficients and diagram. Also, frequency adjustability is achieved by connecting the varactor diode to the structure's resonator. The proposed structure can be used in the frequency range of 1.6–2.2 GHz. Furthermore, the measured return losses in the stopband and passband are 8 dB and 13 dB, respectively. In this paper, all simulations are performed by ADS software.

1. INTRODUCTION

Diplexer is a key component in many microwave communication systems such as wireless communication systems, radar systems, cell phones, and satellite communication systems. On the other hand, it is applied to select or limit signals in many microwave applications for a certain spectral range. Diplexer has three ports that can separate different frequency bands. It also offers other applications of filters. This circuit is obtained by connecting two filters with different central frequencies. Hence, one antenna can be recruited simultaneously as transmitter and receiver in different frequency bands. Diplexer is a useful analogue element in the initial part of telecommunication systems.

As depicted in Fig. 1, the diplexer is located between the antenna and radio frequency section (receiver and transmitter). In various parts of telecommunication systems, conventional microwave diplexers have improper return loss (0 dB) in the stop frequency band which causes unwanted signals in the receiver. This also results in reduced dynamic range and instability of telecommunication (not used in high-density environments) [1]. Moreover, powerful amplifiers recruited in military and commercial radars, earth-based television broadcasting stations, and satellites that are connected to these types of diplexers suffer physical damage and malfunction in the long run due to the out-of-band power return. Due to the reflectionless structures' property which has an appropriate amount of return loss in the stopband, the previous problems can be modified by these structures. The coupling matrix is a theoretical design method for implementing the mentioned structure [2].

In [3], a fully tunable reflectionless bandstop filter using multi-section L-resonators in c band is presented. Also the design methods for first-order reflectionless lumped-element lowpass and bandpass filters are discussed in [4]. In addition, several methods for designing the reflection less filters have been reported in [5–7].

All the mentioned papers are about designing the filters but in this paper, design and fabrication of an adjustable reflectionless microstrip diplexer are presented and discussed.

Received 12 September 2022, Accepted 3 November 2022, Scheduled 10 November 2022
* Corresponding author: Reza Bayderkhani (reza.bayderkhani@iau.ac.ir).
The authors are with the Department of Electrical and Computer Engineering, Islamic Azad University Central, Tehran, Iran.

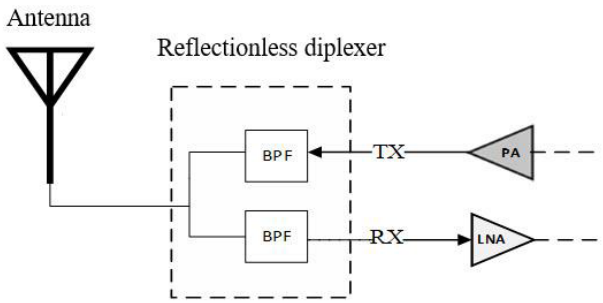

Figure 1. Place of reflectionless diplexer application in a telecommunication system.

2. STRUCTURE

To implement the original design, we first design and analyze two reflectionless L-band bandpass filters with a central frequency 1.6–2.2 GHz based on microstrip transmission lines and half-wavelength resonators.

Then, the quarter length converter is used to connect these two bandpass filters. Finally, we propose the reflectionless diplexer structure with the adjustability of the channel's central frequency. Note that adjustability of the channel's central frequency (bandpass filters) can be achieved by varactor diode in a diplexer circuit. According to [8], the coupling diagram is used to implement the proposed structure's bandpass filters. Fig. 2 illustrates the K-order reflectionless coupling filters diagram.

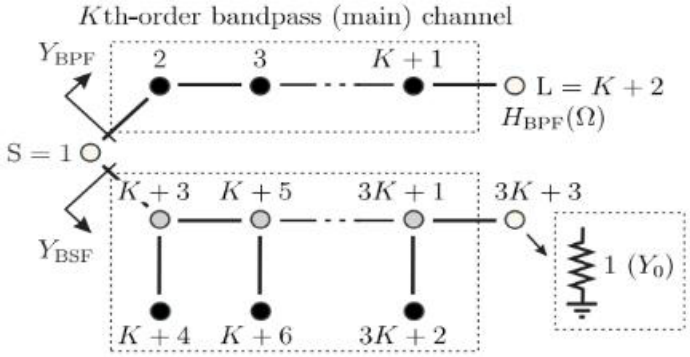

Figure 2. The reflectionless coupling bandpass filter diagram [8].

As shown in Fig. 2, the diagram generally has two paths. The upper and lower paths are respectively the bandpass and bandstop filters' channels. The bandstop filter channel of the two paths is designed with the lines' impedance Z_r as 25–100 Ω. We add the electrical lengths of 90 and 180 degrees phases to these paths' nodes to create zero in the main operation of the circuit. Note that the length and Z_r are proportional to the central frequency and bandwidth, respectively [11, 12]. Due to the main structure coupling between the lines' impedance and the side arms, the parameter M is defined as a coupling coefficient whose lower indices represent the initial and final nodes. Table 1 shows the formula for calculating the coupling coefficient of the reflectionless K-order bandpass and bandstop filters structure. From the coupling coefficient, Equation (1) can be recruited to calculate the impedances of the main structure lines.

The electrical length of all lines in the main path and side arms is calculated according to the central frequency (2 GHz) and 90 degree phase [10].

$$Z_{i,j} = \frac{Z_0}{M_{i,j}} \tag{1}$$

Z_0: Characteristic impedance = 50 Ω.

3. DESIGN, SIMULATION AND RESULTS

To verify the above-mentioned diplexer design theory, the schematic of the diplexer channel (bandpass filter) is designed and shown in Fig. 3. First of all, a bandpass filter (as the diplexer channel) having reflective or reflectionless characteristic is designed. The characteristics of the proposed design such as the initial values of the impedance, coupling coefficient, and central frequency are assumed as follows

$$Z_r = 25\,\Omega,\ \ Z_0 = 50\,\Omega,\ \ K = 3,\ \ f_c = 2\,\text{GHz}$$
$$M_{6,8} = 1,\ \ M_{8,10} = 1,\ \ M_{10,12} = 1,\ \ M_{10,11} = 1$$

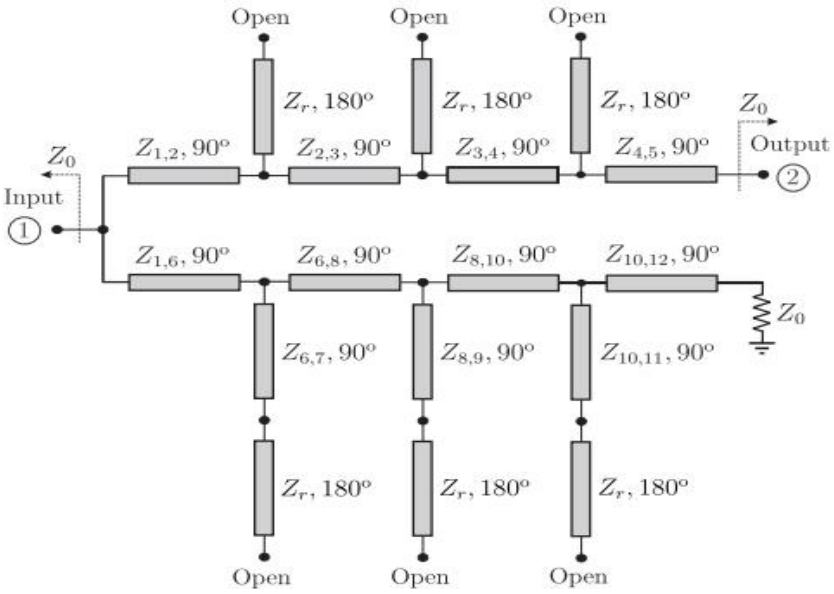

Figure 3. The schematic of the L-band reflectionless bandpass filter.

Due to the above values and Equation (1), the impedance values corresponding to the coupling coefficient of the reflectionless filter structure (third column of Table 1) are calculated as

$$Z_{1,2} = 86.59\,\Omega,\ \ Z_{2,3} = 141.4\,\Omega$$
$$Z_{3,4} = 81.86\,\Omega,\ \ Z_{4,5} = 50\,\Omega,\ \ Z_{1,6} = 50\,\Omega,$$
$$Z_{6,7} = 57.7\,\Omega,\ \ Z_{6,8} = 50\,\Omega,\ \ Z_{8,9} = 61.24\,\Omega,$$
$$Z_{8,10} = 50\,\Omega,\ \ Z_{10,11} = 100\,\Omega,\ \ Z_{10,12} = 50\,\Omega$$

Owing to the type of implementation (microstrip lines) and printed structure's lines (diplexer, filters), the impedance values should be converted to physical values.

For implementation, a Rogers-4003c substrate with the following specifications was recruited: relative dielectric constant 3.38, substrate thickness 0.508 mm, copper thickness 35 μm, and loss tangent 0.0027. From the substrate characteristics and impedance values, the thickness and electrical length values of each structure element are calculated.

Figure 4 shows the simulation of the reflectionless bandpass filter with central frequency 2 GHz. Here, the amount of return loss in the stopband of the bandpass filter is 8 dB, while this value in conventional filters is zero. For this reason, they are called reflectionless filters. By changing the operating frequency in the calculations from 2 to 1.6 GHz, the second channel can also be implemented according to the first channel. To avoid duplication, the values of the elements and frequency response are ignored.

After design and simulation, we connect the two types of reflectionless bandpass filters (that determine the frequency of the original diplexer channels) by quadratic wavelength converter relations

Table 1. Coupling coefficient of the reflectionless three order bandpass filter structure [8].

Order (K)	3
Variables of freedom	$M_{6,8}^{(*)}$, $M_{8,10}^{(*)}$, $M_{10,11}$, $M_{10,12}$
Design formulas	$M_{1,2} = \pm\left(\frac{2}{\sqrt{3}}\right)\left\lvert\frac{M_{10,11}}{M_{10,12}}\right\rvert$, $M_{2,3} = \pm\sqrt{2}\,\frac{M_{10,11}^2}{M_{10,12}^2}$, $M_{3,4} = \pm\frac{\sqrt{6}M_{10,11}^2}{M_{10,12}^2}$, $M_{4,5} = \pm 2\left\lvert\frac{M_{10,11}}{M_{10,12}}\right\rvert$, $M_{1,6} = \pm\left\lvert\frac{M_{6,8}M_{10,12}}{M_{8,10}}\right\rvert$, $M_{6,7} = \pm\sqrt{3}\left\lvert\frac{M_{6,8}M_{10,11}}{M_{8,10}}\right\rvert$, $M_{8,9} = \pm 2\sqrt{2/3}\,\frac{\lvert M_{8,10}M_{10,11}\rvert}{M_{10,12}^2}$

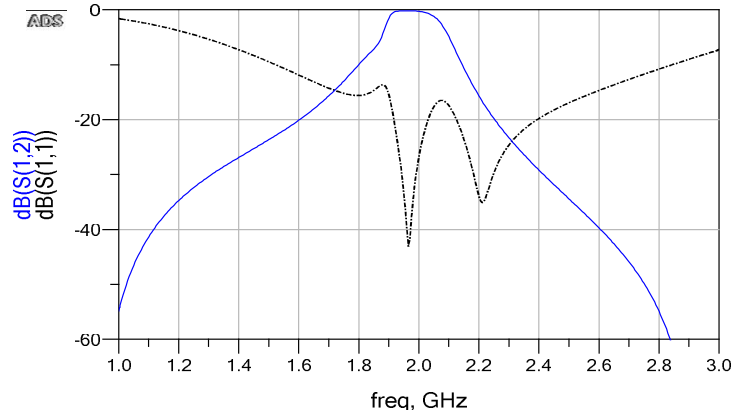

Figure 4. Simulation results of the L-band reflectionless diplexer's first channel (bandpass filter).

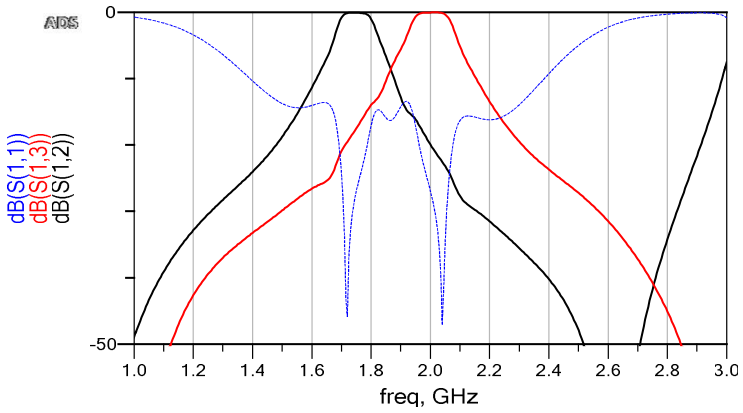

Figure 5. Complete simulation results of the L-band reflectionless diplexer.

and form the original structure of the L-band reflectionless diplexer. Fig. 5 displays the complete simulation results of the L-band reflectionless diplexer by observing the mentioned items. Each response of these channels must have a high impedance at the central frequency of the other channel so that the signal does not pass through it.

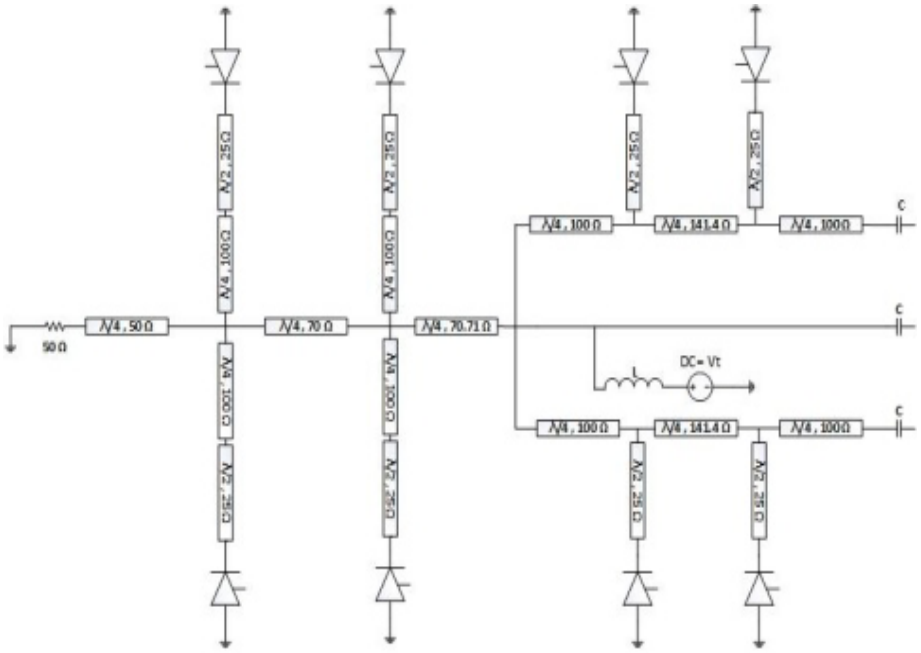

Figure 6. The general structure of tunable L-band reflectionless diplexer.

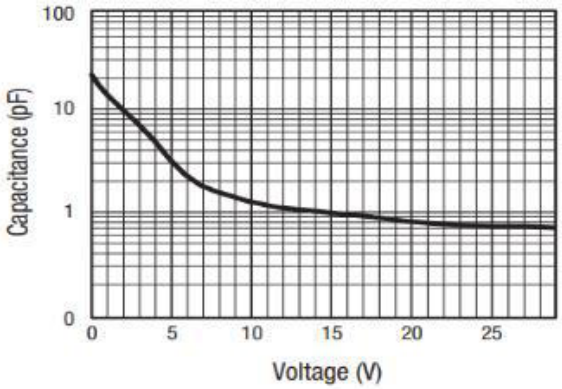

Figure 7. Capacitance versus applied voltage [9].

With the formation of the main diplexer structure, the return loss values in passband and stopband are 17 dB and 8 dB, respectively. The insertion loss of 0.2 dB and the bandwidth of 9.8% relative to the central frequency can be seen in the simulation results. So far, we have analyzed the design and implementation of the L-band reflectionless diplexer.

For a tunable structure, the central frequency of the channels can be shifted without any major conversion (up and down). Hence, the main structure resonators' frequency (open circuit stubs of each circuit branch) must be changed by altering the capacitance. The capacitance value can be changed by an element such as a variable capacitor or varactor diode and cause the frequency shift in structure. In this study, we change the capacitance by the DC voltage applied to the varactor diode with part number SMV1265-040LF which is connected between the ground circuit and the end of the structure stubs. The general structure of a tunable L-band reflectionless diplexer is shown in Fig. 6. For this type of structure, AC and DC analysis must be performed regarding the used diode reverse voltage.

Since the limiting element in the design is the varactor diode SMV1265, we cannot optimize the capacitance. In other words, the design frequency response should be evaluated and analysed in proportion to the capacity of 1 pF to 10 pF. Fig. 7 demonstrates the capacitance versus the diode

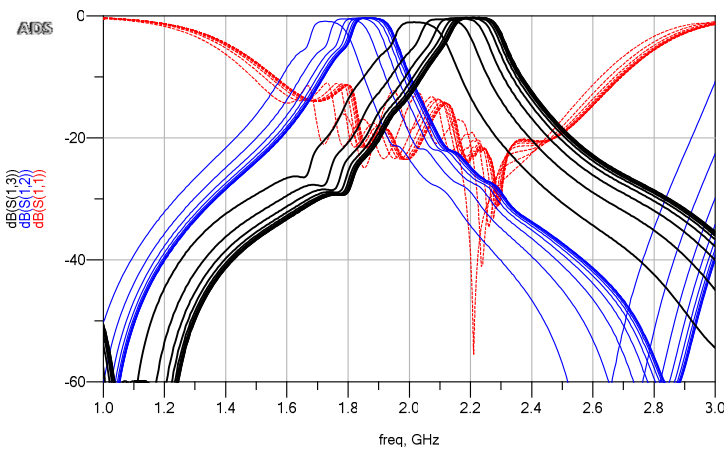

Figure 8. Simulation results of tunable L-band reflectionless diplexer for all voltages.

Table 2. Simulation results values of tunable L-band reflectionless diplexer for different voltages.

Voltage	Channel frequency (GHz)		Insertion loss		Return loss	
	First channel	Second channel	First channel	Second channel	Passband	Stopband
7 volts	1.65	1.95	1.3	1.5	17	12
16 volts	1.85	2.18	0.5	0.7	19	13
20 volts	1.87	2.2	0.5	0.7	18	13

reverse voltage.

To DC analyse the structure, we must enter the parameters of the SPICE model of the diode SMV1265 in ADS software from the technical specifications.

By placing the complete diode model, the frequency responses are simulated for different applied DC voltages such as 7 v, 16 v, and 20 v in Fig. 8. The extracted electrical characteristics from the simulation results are recorded in Table 2.

Due to the limitation on the used varactor diode, the change rate of central frequency at voltages 12 volts upwards is low and insignificant compared to the lower voltages. From Fig. 7, this behavior was predictable because the capacitance does not change much from this threshold level upwards.

According to the circuit structure in Fig. 6, we need the DC voltages from 8 to 24 volts to bias the varactor diodes. These voltages are applied to the circuit from the external power supply. The RF-chock inductor must have a large impedance at the circuit operating frequency. Initially, the input and output ports contained a capacitor that acts as a DC-Block. The used capacitor and inductor must not affect the AC circuit at the lowest circuit operating frequency. The use of DC-Block in the input and output sections is mandatory because the DC circuit response may change when being connected to other circuits or network analyzer. In addition to the RF-chock inductor, a high resistor (10 kΩ) can be used to benefit advantages such as reduced current consumption and lack of effect on the AC circuit.

For testing each route, the other route must match the load 50 Ω. To prevent current from flowing through the resistor, we must replace it with a large capacitor so that the current consumption of the circuit is reduced, the DC equivalent structure not changed, and the response not affected. In accordance with Fig. 9 and observing the mentioned considerations, we proceed to the assembly of SMA circuit elements and connectors.

Comparison of the full frequency response of the structure in both simulated and measured quantities by Keysight N9918A Analyzer Network is shown in Figs. 10, 11, and 12. The return loss of the first port and the insertion losses of the second and third ports are respectively shown in Figs. 10, 11, and 12.

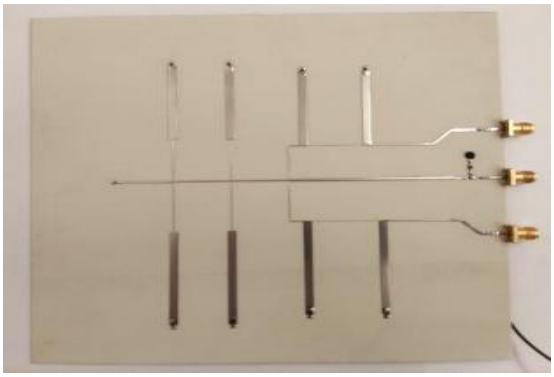

Figure 9. Construction model of tunable L-band reflectionless.

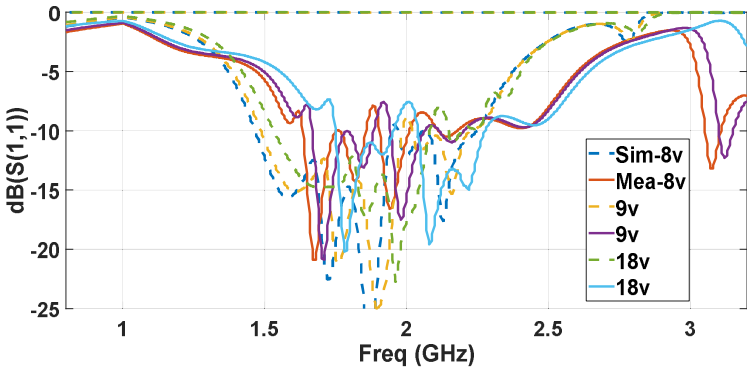

Figure 10. The simulated and measured return loss response for tunable L-band reflectionless diplexer.

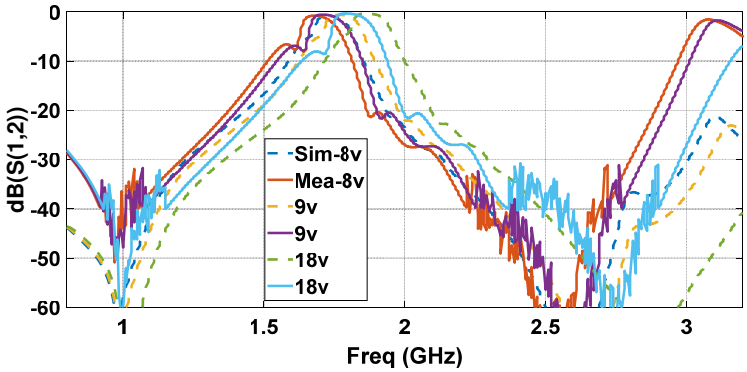

Figure 11. Comparison of the simulated and measured response of the first channel in tunable L-band reflectionless diplexer.

As can be seen, the simulation and measurement results are different in parts such as channel frequency and insertion loss. Also, the 105 MHz downshift of channel frequencies can be attributed to the errors in the printed circuit structure and substrate manufacturer. On the other hand, channels insertion loss increases due to the use of an improper DC-Block capacitor, which causes a loss about 0.5 dB in the passband.

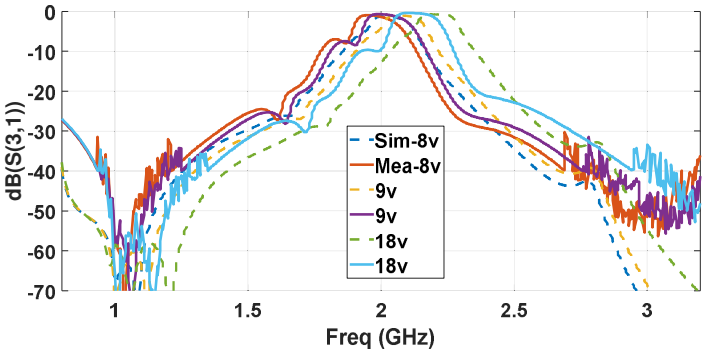

Figure 12. Comparison of the simulated and measured response of the second channel in tunable L-band reflectionless diplexer.

Table 3. Comparison of proposed reflectionless diplexer with conventional diplexers.

References	Channel Frequency (GHz)	Proportional Bandwidth (%)	Insertion Loss (dB)	Return Loss in Passband (dB)	Return Loss in Stopband (dB)	Isolation (dB)
[5]	2.45 5.35	13.2 17.8	0.2 0.5	15	0	20
[6]	2.40 5.21	8.1 4.4	0.9 1.2	28	0	23
[7]	2.45 3.5	4 5.7	1.4 1.3	20	0	35
Proposed structure	1.6–2.2	9.3 8.4	0.5	13	8	18

4. CONCLUSION

Due to the novelty of the reflectionless structure's topic, there is no benchmark for proper comparison. Therefore, Table 3 has been completed with the accomplished studies' priority in the L-band (articles, conferences, etc.) to review and evaluate the proposed structure.

REFERENCES

1. Morgan, M. A., *Reflectionless Filters*, Artech House, 2017.
2. Morgan, M. A. and T. A. Boyd, "Theoretical and experimental study of a new class of reflectionless filter," *IEEE Transactions on Microwave Theory and Techniques*, Vol. 59, No. 5, 1214–1221, 2011.
3. Chieh, J.-C. S. and J. Rowland, "A fully tunable C-band reflectionless bandstop filter using L-resonators," *2016 46th European Microwave Conference (EuMC)*, 131–133, 2016, doi: 10.1109/EuMC.2016.7824295.
4. Lee, T.-H., B. Lee, and J. Lee, "First-order reflectionless lumped-element lowpass filter (LPF) and bandpass filter (BPF) design," *2016 IEEE MTT-S International Microwave Symposium (IMS)*, 1–4, 2016, doi: 10.1109/MWSYM.2016.7540235.
5. Yang, L., R. Gómez-García, J.-M. Muñoz-Ferreras, R. Zhang, D. Peroulis, and L. Zhu, "Multilayered reflectionless wideband bandpass filters with shunt/in-series resistively terminated microstrip lines," *IEEE Transactions on Microwave Theory and Techniques*, Vol. 68, No. 3, 877–893, March 2020, doi: 10.1109/TMTT.2019.2952861.

6. Lee, J., B. Lee, S. Nam, and J. Lee, "Topology and rigorous design method for reflectionless bandstop filter," *2019 49th European Microwave Conference (EuMC)*, 456–459, 2019, doi: 10.23919/EuMC.2019.8910927.
7. Psychogiou, D. and R. Gómez-García, "Tunable reflectionless microstrip bandpass filters," *2018 IEEE Radio and Wireless Symposium (RWS)*, 49–51, 2018, doi: 10.1109/RWS.2018.8304943.
8. Gomez-Garcia, R., J.-M. Munoz-Ferreras, and D. Psychogiou, "High-order input-reflectionless bandpass/bandstop filters and multiplexers," *IEEE Transactions on Microwave Theory and Techniques*, Vol. 67, No. 9, 3683–3695, 2019.
9. Cameron, R. J., C. M. Kudsia, and R. R. Mansour, *Microwave Filters for Communication Systems: Fundamentals, Design, and Applications*, John Wiley & Sons, 2018.
10. Chinig, A., et al., "A new microstrip diplexer using open-loop resonators," *Journal of Microwaves, Optoelectronics and Electromagnetic Applications*, Vol. 13, No. 2, 185–196, 2014.
11. Zhu, C., L. Yao, and J. Zhou, "Novel microstrip diplexer based on a dual-band bandpass filter for WLAN system," *IEEE 2010 Asia-Pacific Microwave Conference*, 1102–1105, 2010.
12. Tantiviwat, S., N. Intarawiset, and R. Jeenawong, "Wide-stopband, compact microstrip diplexer with common resonator using stepped-impedance resonators," *IEEE 2013 Tencon-Spring*, 174–177, 2013.